# Cytoplasmic Control of Sense-Antisense mRNA Pairs

Flore Sinturel, Albertas Navickas, Maxime Wery, Marc Descrimes, Antonin
Morillon, Claire Torchet, Lionel Benard

## HAL Id: hal-01216461
## https://hal.sorbonne-universite.fr/hal-01216461

Submitted on 16 Oct 2015

# Cytoplasmic Control of Sense-Antisense mRNA Pairs

## Graphical Abstract
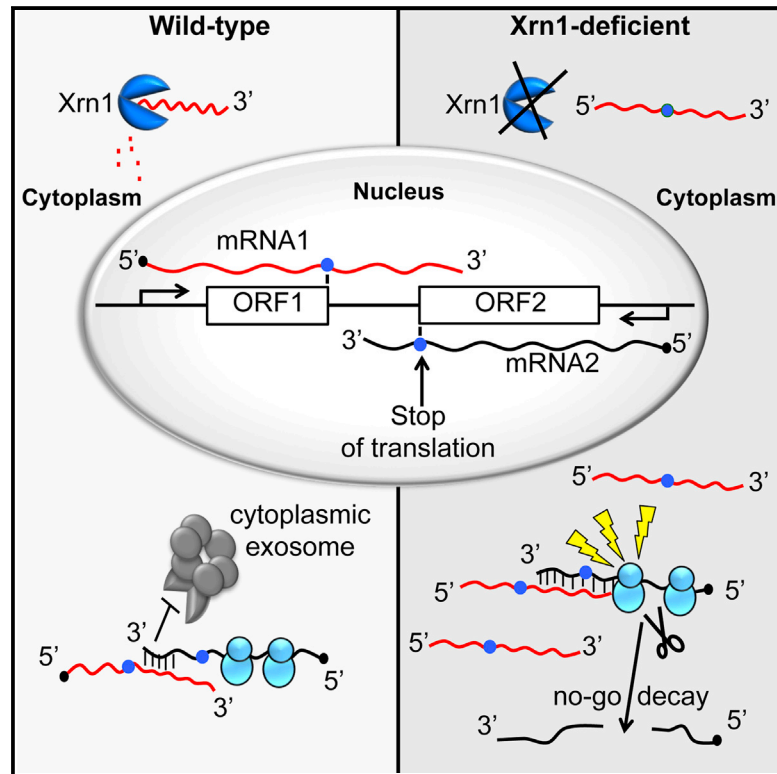


## Highlights

- Transcription of convergent coding genes can form mRNA-mRNA duplexes

- Cytoplasmic mRNA-mRNA interaction can trigger no-go decay or limit 3′-5′ degradation

- Hundreds of mRNA-mRNA interactions are characterized in wild-type cells

- mRNA-mRNA interactions are subjected to surveillance by Xrn1

## Authors

Flore Sinturel, Albertas Navickas, Maxime Wery, ..., Antonin Morillon, Claire Torchet, Lionel Benard

## Correspondence

antonin.morillon@curie.fr (A.M.), lionel.benard@ibpc.fr (L.B.)

## In Brief

Sinturel et al. demonstrate that the complementary tails of 3′-overlapping mRNAs can interact in the cytoplasm and promote post-transcriptional regulatory events. They show that hundreds of mRNA-mRNA interactions exist in wild-type cells and are controlled by Xrn1, a conserved 5′-3′ cytoplasmic exoribonuclease in eukaryotes.

## Accession Numbers

GSE64090

# Cytoplasmic Control of Sense-Antisense mRNA Pairs

Flore Sinturel,[1,3,4] Albertas Navickas,[1,4] Maxime Wery,[2] Marc Descrimes,[2] Antonin Morillon,[2,*] Claire Torchet,[1] and Lionel Benard[1,*]

[1]Sorbonne Universités, UPMC Paris 06, CNRS UMR8226, Laboratoire de Biologie Moléculaire et Cellulaire des Eucaryotes, Institut de Biologie Physico-Chimique, 75005 Paris, France
[2]Institut Curie, PSL Research University, CNRS UMR3244, Université Pierre et Marie Curie, 26 rue d'Ulm, 75248 Paris Cedex 05, France
[3]Present address: Department of Molecular Biology, Sciences III, University of Geneva, 1211 Geneva, Switzerland
[4]Co-first author
*Correspondence: antonin.morillon@curie.fr (A.M.), lionel.benard@ibpc.fr (L.B.)
http://dx.doi.org/10.1016/j.celrep.2015.08.016

## SUMMARY

Transcriptome analyses have revealed that convergent gene transcription can produce many 3′-overlapping mRNAs in diverse organisms. Few studies have examined the fate of 3′-complementary mRNAs in double-stranded RNA-dependent nuclear phenomena, and nothing is known about the cytoplasmic destiny of 3′-overlapping messengers or their impact on gene expression. Here, we demonstrate that the complementary tails of 3′-overlapping mRNAs can interact in the cytoplasm and promote post-transcriptional regulatory events including no-go decay (NGD) in *Saccharomyces cerevisiae*. Genome-wide experiments confirm that these messenger-interacting mRNAs (mimRNAs) form RNA duplexes in wild-type cells and thus have potential roles in modulating the mRNA levels of their convergent gene pattern under different growth conditions. We show that the post-transcriptional fate of hundreds of mimRNAs is controlled by Xrn1, revealing the extent to which this conserved 5′-3′ cytoplasmic exoribonuclease plays an unexpected but key role in the post-transcriptional control of convergent gene expression.

## INTRODUCTION

In many species of vertebrates, invertebrates, plants, and yeast (Djebali et al., 2012; Kapranov et al., 2007; Katayama et al., 2005; Li et al., 2008; Pelechano et al., 2013; Wang et al., 2005; Zhang et al., 2006), genomic loci produce oppositely oriented transcripts that overlap. Analyses of sense and antisense transcripts produced by convergent transcription have focused on coding/non-coding RNA pairs that are prevalent in databases. This has highlighted the importance of non-coding RNAs (ncRNAs) in the regulation of many biological processes, including siRNA-induced gene silencing, cis-RNA-mediated chromatin modifications, transcriptional interference, or RNA editing (Faghihi and Wahlestedt, 2009;

Jacquier, 2009; Ponting et al., 2009; Pelechano and Steinmetz, 2013).

Transcriptome analyses have additionally shown that convergent gene transcription can produce tail-to-tail 3′-overlapping mRNA pairs in eukaryotes (Djebali et al., 2012; Faghihi and Wahlestedt, 2009; Jen et al., 2005; Kapranov et al., 2007; Katayama et al., 2005; Lapidot and Pilpel, 2006; Li et al., 2008; Munroe and Zhu, 2006; Pelechano et al., 2013; Wang et al., 2005; Wilkening et al., 2013; Yelin et al., 2003; Zhang et al., 2006), but surprisingly few examples exist where sense-antisense mRNA pairs have been shown to form mRNA duplexes with regulatory consequences. One precedent for a potential mRNA duplex can be found in *Arabidopsis thaliana* and concerns the SRO5-P5CDH sense-antisense messenger pair, proposed to be processed into natural siRNAs that could participate in the response to salt stress (Borsani et al., 2005). Remarkably, transcriptome analysis of *A. thaliana* reveals the existence of at least 1,000 of convergent and overlapping coding gene pairs, constituting an immense unexplored reservoir of potential mRNA duplexes (Jen et al., 2005). A study in human cells correlated the expression of the RevErb messenger to the regulation of erbAα2 mRNA splicing (Hastings et al., 1997; Salato et al., 2010) via an mRNA-mRNA interaction. In this case, at least 600 additional overlapping coding genes have been identified (Sanna et al., 2008).

We wished to address the question of the fate of 3′-overlapping messengers in the model organism *Saccharomyces cerevisiae*, where hundreds of 3′-overlapping mRNA result from convergent gene transcription and can theoretically form mRNA duplexes (Pelechano et al., 2013; Wilkening et al., 2013). Convergent gene expression has already been shown to lead to transcriptional interference in *S. cerevisiae*. Indeed, using artificial constructs, Prescott and Proudfoot (2002) demonstrated that convergent transcription can result in the collision of RNA polymerases. These collisions led to a reduction in transcription of both genes and limited the production of 3′-overlapping transcripts (Prescott and Proudfoot, 2002). Here, we focus on the post-transcriptional cytoplasmic fate of natural 3′-overlapping mRNAs resulting from convergent gene transcription (Pelechano et al., 2013).

Our first indication of the potential existence of messenger-interacting mRNAs (mimRNAs) came from our previous work demonstrating the importance of Xrn1 for respiration in *S. cerevisiae* (Sinturel et al., 2012). Xrn1 encodes a cytoplasmic
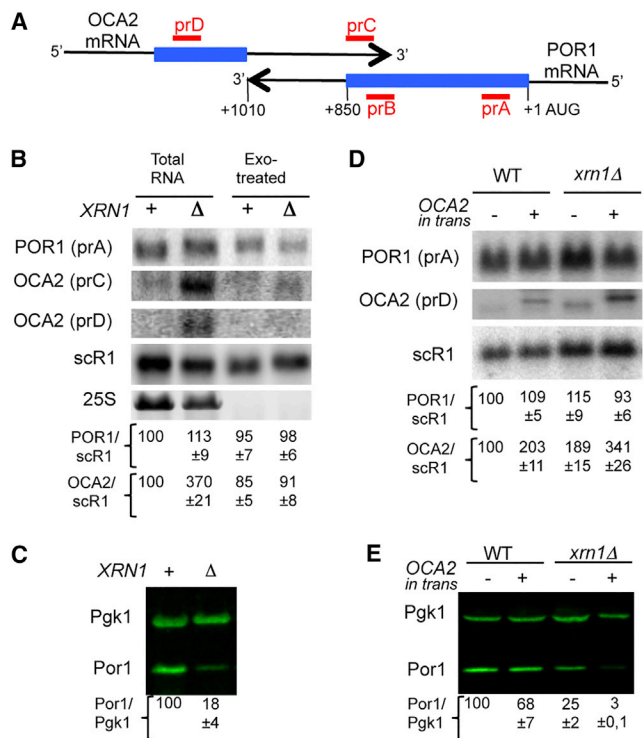
**Figure 1. Expression of OCA2 mRNA in *trans* Affects Por1 Protein Production**

(A) Schematic of POR1 and OCA2 mRNAs showing the extent of overlap in their 3′ regions. Filled boxes indicate open reading frames, and black arrows represent 3′ UTRs. Probes prA, prB, prC, and prD used in northern blots analysis are indicated in red.

(B) Northern blot showing steady-state levels of POR1 and OCA2 mRNA in wild-type and *xrn1Δ* strains. Total RNA and total RNA treated with Xrn1 in vitro (Exo-treated) to deplete 5′-monophosphorylated RNA (i.e., 5′-decapped RNAs) are shown. The 25S rRNA has 5′ monophosphate group and serves as a positive control for exonucleolytic digestion. The scR1 RNA (a PolIII transcript insensitive to exoribonuclease treatment) served as a loading control. Quantifications of RNAs relative to scR1, before or after 5′-3′ exoribonuclease treatment, are indicated below the blots (quantification of the OCA2 mRNA was done using prD).

(C) Western blot of Por1 protein in wild-type and *xrn1Δ* strains. Pgk1 was used as a loading control. Quantifications of Por1 relative to Pgk1 are indicated below the blot.

(D) Northern blot analysis of POR1 mRNA steady-state levels upon expression (+) or not (−) of OCA2 mRNA in *trans*. Differences in OCA2 mRNA size are due to *OCA2* expression from a plasmid borne *CYC1* promoter that extends the 5′ UTR sequence by 132 nucleotides (see Experimental Procedures).

(E) Western blot analysis performed as in (D) upon expression (+) or not (−) of OCA2 mRNA in *trans*. All northern and western blot quantifications are indicated with SEs calculated from at least three independent experiments.

5′-3′ exoribonuclease activity that is evolutionarily conserved. It is also known for the direct or indirect pleiotropic cellular defects correlated with its inactivation in all eukaryotes where it has been examined (Nagarajan et al., 2013). As a first step, we analyzed a specifically affected gene, *POR1*, encoding the mitochondrial porin Por1 and demonstrate that mRNA-mRNA interactions with the 3′-overlapping OCA2 mRNA in an *xrn1* mutant strain are responsible for the functional inactivation of the POR1 mRNA at a post-transcriptional level. Indeed, we demonstrate

that this overlap can inhibit ribosome translocation and trigger an endoribonucleolytic cleavage characteristic of the no-go decay (NGD) pathway (Doma and Parker, 2007). In wild-type cells, we observe that the POR1-OCA2 interaction interferes with 3′-5′ mRNA decay, showing that these RNA-RNA interactions also have biological consequences in the presence of Xrn1 (Anderson and Parker, 1998). Finally, we demonstrate that hundreds of mimRNAs exist in *S. cerevisiae* and that most of these are controlled by Xrn1.

## RESULTS

### Regulation of POR1 Expression by OCA2 mRNA in *trans*

Our previous work demonstrated the importance of the cytoplasmic 5′-3′ exoribonuclease activity of Xrn1 for the expression of *POR1*, which encodes the mitochondrial porin in *S. cerevisiae* (Figure 1A) (Sinturel et al., 2012). In the absence of Xrn1, Por1 protein levels are decreased several-fold. This observation could not be explained by the presence of Xrn1-sensitive unstable transcripts (XUTs) (van Dijk et al., 2011) in the vicinity of *POR1* as none were detectable by extensive RT-PCR experiments or northern blot analyses (data not shown). On the other hand, increased levels of an antisense mRNA originating from the *OCA2* gene on the opposite strand were detected in *xrn1* mutant strains (Figure 1B). An overlap between the 3′ regions of the OCA2 and POR1 mRNAs was seen in sequencing analyses (Pelechano et al., 2013). Using Por1-specific antibodies, we confirmed that Por1 was less abundant at the protein level in the *xrn1* mutant whereas the quantity of POR1 mRNA did not vary (Figures 1B and 1C). The increase in OCA2 RNA levels in the *xrn1* mutant strain suggested that this RNA is a potential target for Xrn1 degradation, as is the case for many cellular mRNAs (He et al., 2003; van Dijk et al., 2011). In vitro treatment of total RNA with Xrn1 (which only attacks 5′-monophosphory-lated RNA) resulted in decreased OCA2 mRNA levels whereas the POR1 mRNA levels were unaffected (Figure 1B). Because Xrn1 cannot degrade capped RNA (Nagarajan et al., 2013), we conclude that the OCA2 mRNA accumulates as a 5′-monophosphorylated RNA in *xrn1Δ* strains.

We also observed that the overexpression of the OCA2 transcript in *trans* from a plasmid was inversely correlated with Por1 protein levels in *xrn1Δ* cells in particular (Figures 1D and 1E). Therefore, the OCA2 mRNA can negatively affect *POR1* expression in *trans*. Interestingly, overexpression of a 5′-truncated OCA2 RNA that overlaps the 3′ region of the POR1 mRNA also resulted in reduced Por1 protein levels (Figures S1A and S1B), excluding the possibility that the Oca2 protein is involved in this regulation. These results suggest that Xrn1 acts on *POR1* expression at a post-transcriptional level through an interaction between the complementary 3′ RNA sequences of the POR1 and OCA2 mRNAs. We therefore define OCA2 and POR1 mRNAs as potential mimRNAs.

### OCA2 mRNA Triggers NGD of POR1 mRNA

Transcriptome analysis suggested that the OCA2 transcript overlaps the POR1 mRNA and extends into the POR1 ORF (Pelechano et al., 2013). This was verified by northern blotting using specific oligonucleotide probes (Figure 1B). To explain the low
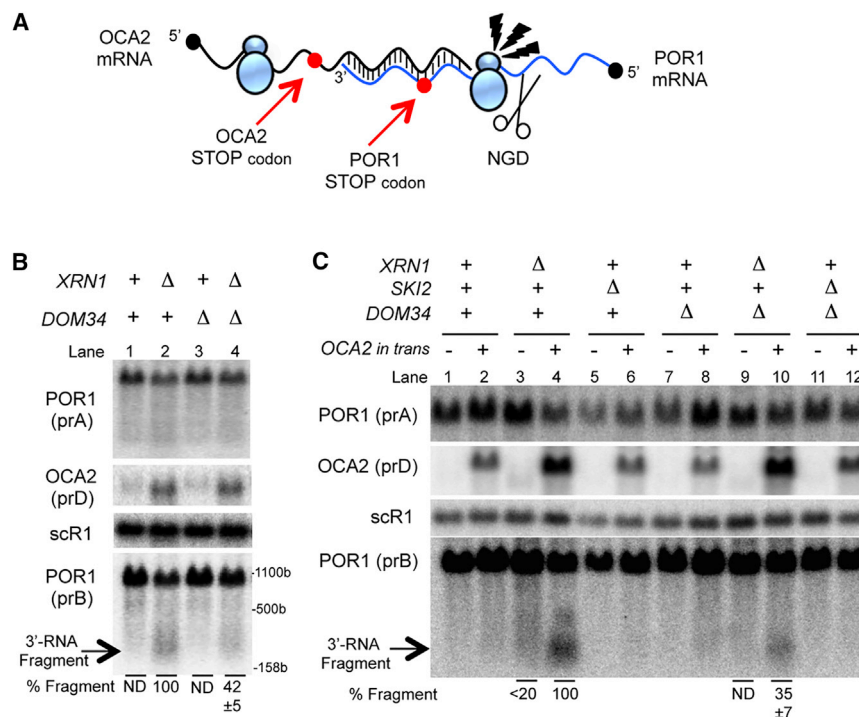
**Figure 2. OCA2 mRNA Expressed in *trans* Triggers No-Go Decay of POR1 mRNA**

(A) Model of NGD of the POR1 mRNA in the presence of the OCA2 transcript. The translational stop codon of POR1 mRNA is indicated by a red circle. The ribosome stall due to the presence of OCA2-POR1 RNA duplex is symbolized by lightning flashes and the subsequent endonucleolytic cleavage (Doma and Parker, 2006) indicated by scissors. Bars indicate the potential interactions between the two RNA sequences.

(B) Detection of the 3′ RNA fragment of POR1 in wild-type, *xrn1Δ*, or/and *dom34Δ* strains by northern blot analysis.

(C) Northern blot analysis in *xrn1Δ*, *ski2Δ*, and *dom34Δ* genetic contexts. Analysis of the production of the POR1 3′-RNA fragment upon expression (+) or not (−) of OCA2 mRNA in *trans*. In (B) and (C), the presence of the 3′ RNA fragment of POR1 is indicated by an arrow. Probes prA, prB, and prD were used in northern blot analysis (see Figure 1). The % fragment is the relative ratio of fragment to full-length POR1 standardized to a percentage of 100% for *xrn1* mutant. All quantifications are indicated with SEs calculated from at least three independent experiments. ND, not determined. The scR1 RNA served as a loading control.

levels of Por1 protein, whereas the corresponding POR1 mRNA levels were unchanged, we considered the possibility that RNA duplex formation between these overlapping RNAs could prevent ribosomes from correctly terminating POR1 mRNA translation (Figure 2A). This model was based on previous work on the PGK1 mRNA with a stem-loop artificially inserted in the coding region (PGK1-SL) that blocks ribosomes and triggers cleavage of the mRNA in a Dom34-dependent manner (Doma and Parker, 2006). The 3′ cleavage fragment of the PGK1-SL mRNA is detectable in an *xrn1* mutant, in which cytoplasmic 5′-3′ exonucleolytic digestion is abolished, and the phenomenon is referred to as NGD (Doma and Parker, 2006; Passos et al., 2009). We thus asked whether the POR1 mRNA base paired with the 3′ end of OCA2 mRNA would be an NGD mRNA target (Figure 2A). Consistent with this idea, we observed an accumulation of a POR1 3′ fragment in *xrn1Δ* strains (Figure 2B, lane 2). We also asked whether the OCA2 mRNA was NGD targeted. Probing this RNA with 5′- or 3′-specific probes revealed a unique full-length mRNA (Figure 1B), and no 3′ RNA fragment was detected (see also Figure S1C). That OCA2 is not a substrate for NGD is consistent with RNA-seq data showing the POR1 mRNA does not overlap with the OCA2 ORF and therefore not likely to impact OCA2 translation (Pelechano et al., 2013). We also observed that steady-state levels of decapped OCA2 mRNA were independent of the presence of POR1 mRNA (Figure S1C), suggesting a limited impact of POR1 mRNA interaction on OCA2 mRNA accumulation.

We observed that POR1 3′ fragment accumulation was even stronger when the OCA2 message was overexpressed in *trans* (Figure 2C, lane 4 versus 3). We also observed that the presence of lithium in the growth medium, which metabolically inhibits the

activity of Xrn1 through the accumulation of pAp in vivo (Dichtl et al., 1997), triggered the production of a POR1 3′ fragment (Figures S2A and S2B). This shows that, in addition to the constitutive surveillance role of Xrn1 in this phenomenon, there are physiological conditions where the activity of Xrn1 becomes critical for avoiding NGD of the POR1 mRNA.

As was observed for the NGD-targeted PGK1-SL mRNA (Doma and Parker, 2006), the detection of the POR1 3′ fragment was dependent on the presence of Dom34, as shown by the reduced levels of this fragment in *dom34Δ xrn1Δ* strains in comparison with *xrn1Δ* strains (in Figure 2B, see lane 4 versus 2, and in Figure 2C, see lane 10 versus 4). As expected, the deletion of *SKI2*, known to inactivate the cytoplasmic 3′-5′ degradation pathway (Anderson and Parker, 1998), had no impact on the detection of this 3′ RNA fragment (Doma and Parker, 2006; Passos et al., 2009) (Figure 2C, lanes 5, 6, 11, and 12).

Additionally, we detected the POR1 RNA 3′ fragment in the monosome- and disome-containing fractions of polysome profiles of Xrn1-deficient cells (see *xrn1Δ* extract in Figure S2D in comparison to WT extract in Figure S2C). RNA-probing experiments also confirmed that these 3′ RNA fragments of POR1 include about 100 nucleotides of the ORF, sufficient to bind one or two ribosomes (Wolin and Walter, 1988) (Figure S2E). In sum, the POR1 3′ fragment has all the characteristics of a NGD product, putatively dependent upon the co-translational interaction with the OCA2 mRNA.

## Sequence-Specific mRNA-mRNA Complementarity Triggers NGD

To validate the hypothesis that mRNA-mRNA interactions are the source of this NGD signal (i.e., that they block ribosome
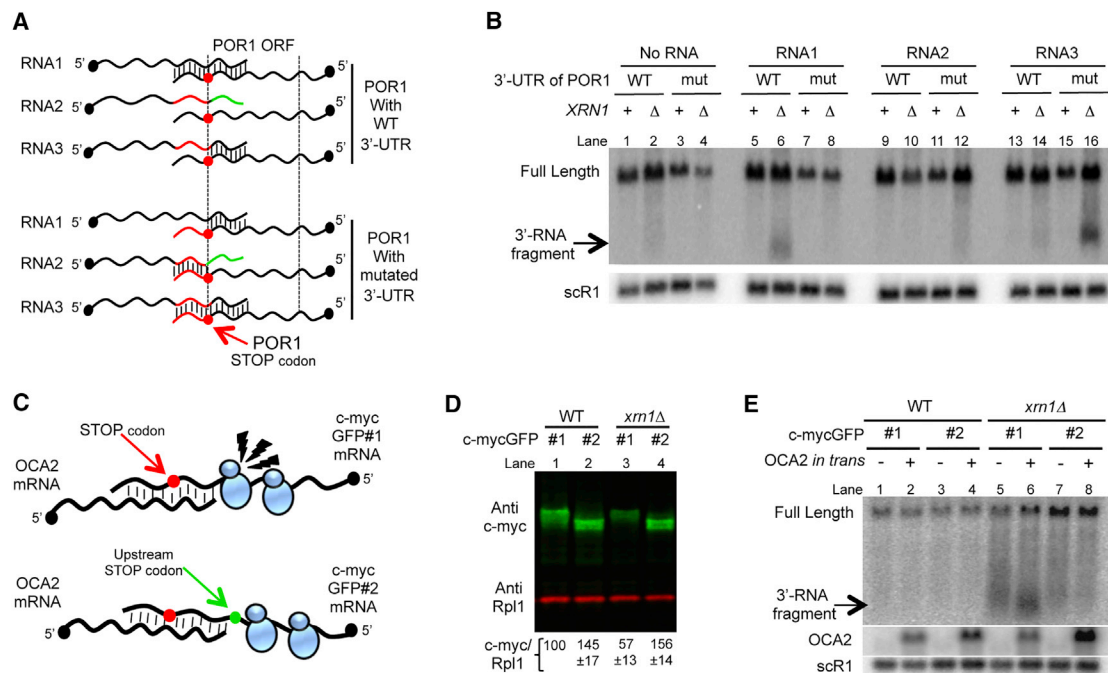
**Figure 3. mRNA-mRNA Interactions Occur In Vivo and Can Induce Cytoplasmic Post-transcriptional Events**

(A) Schematic of RNAs 1, 2, and 3 expressed in *trans* and having putative full, partial, or no complementarity with the wild-type or mutated 3′ UTR region of POR1 mRNAs. Bars indicate the potential interactions between sequences of the two RNAs. The POR1 ORF is delimited by dashed lines. The translational stop codon is indicated by a red circle.

(B) Northern blot analysis of POR1 mRNA with wild-type and mutated 3′ UTR in the presence of RNAs 1, 2, or 3 expressed in *trans*. Probe prB is designed for the detection of the 3′ RNA fragment that can be produced by both wild-type and modified POR1 mRNAs. The production of a 3′ RNA fragment of POR1, indicated by an arrow, is analyzed in the presence or absence (no RNA) of RNA1, 2, or 3 expressed in *trans*. WT and mut specify the nature of the 3′ UTR of POR1 mRNA analyzed, wild-type 3′ UTR, and mutated 3′ UTR, respectively. The scR1 RNA served as a loading control.

(C) Schematic of c-mycGFP no. 1 mRNA reporter expressed from a c-*myc*-tagged *GFP* integrated in the *POR1* gene. The overlap between the OCA2 and POR1 mRNAs is conserved in these constructs, but c-mycGFP no. 2 mRNA differs from c-mycGFP no. 1 mRNA only by an additional stop codon (indicated by a green circle) inserted upstream of the RNA duplex containing the normal stop codon (red circle). Lightning flashes represent the clash between elongating ribosomes and the RNA duplex formed on c-mycGFP no. 1.

(D) Western blot analysis of c-mycGFP no. 1 (#1) and c-mycGFP no. 2 (#2) tagged proteins in wild-type and *xrn1Δ* strains. Rpl1 was used as a loading control, and quantifications of c-*myc* relative to Rpl1 are indicated below with SEs calculated from at least three independent experiments.

(E) Northern blot analysis of c-mycGFP no. 1 (#1) and c-mycGFP no. 2 mRNAs (#2) upon expression (+) or not (−) of OCA2 mRNA in *trans* in the wild-type or in the *xrn1* mutant. The probe prB is designed for the detection of a 3′ RNA fragment (indicated by an arrow) produced by either mRNA no. 1 or no. 2.

translocation), we further studied the accumulation of POR1 3′ RNA fragments in strains expressing POR1 mRNAs with different 3′ UTRs upon overproduction of artificial transcripts with or without complementarity to the 3′ coding sequence and 3′ UTR of POR1 (Figure 3A). For instance, RNA1 was designed to have full complementarity (3′ coding sequence plus 3′ UTR) to the POR1 mRNA and partial complementarity to the POR1 mRNA with a mutated 3′ UTR. Conversely, RNA3 was designed to have full complementarity to the mutated 3′ UTR POR1 mRNA and partial complementarity to WT POR1 mRNA (Figure 3A). RNA2 has no complementarity to the WT 3′ UTR POR1 mRNA and only has complementarity to the mutated 3′ UTR POR1 mRNA. Theoretically, RNA2 can interact with the mutated 3′ UTR POR1 mRNA but cannot block ribosome translocation. The results shown in Figure 3B revealed that only a full complementarity between the 3′ region of the two transcripts produced a POR1 3′ RNA fragment (Figure 3B, see lane 6, showing the WT 3′ UTR POR1 mRNA in the presence of RNA1, or lane 16,

showing the mutated 3′ UTR POR1 mRNA in the presence of RNA3).

According to the NGD model, these mRNA-mRNA interactions are likely to instigate a pausing of ribosomes before they terminate translation. To test this idea, we constructed a c-*myc*-tagged GFP-POR1 fusion, c-mycGFP no. 1 as a Por1 reporter, and made a second construct in which the unique modification was to displace the site of translation termination upstream of the potential RNA duplex, a construct called c-mycGFP no. 2 (Figure 3C). As expected, the expression of the Por1 reporter, c-mycGFP no. 1, was repressed in the *xrn1* mutant (Figure 3D, lane 3 versus 1), whereas the expression of the c-mycGFP no. 2 construct was Xrn1-independent (Figure 3D, lane 4 versus 2). Presumably, the upstream translation termination site inserted in the c-mycGFP no. 2 mRNA facilitates translation termination independently of the formation of the RNA duplex downstream. In accordance with the idea that elongating ribosomes clash with the RNA duplexes, northern blots assays for
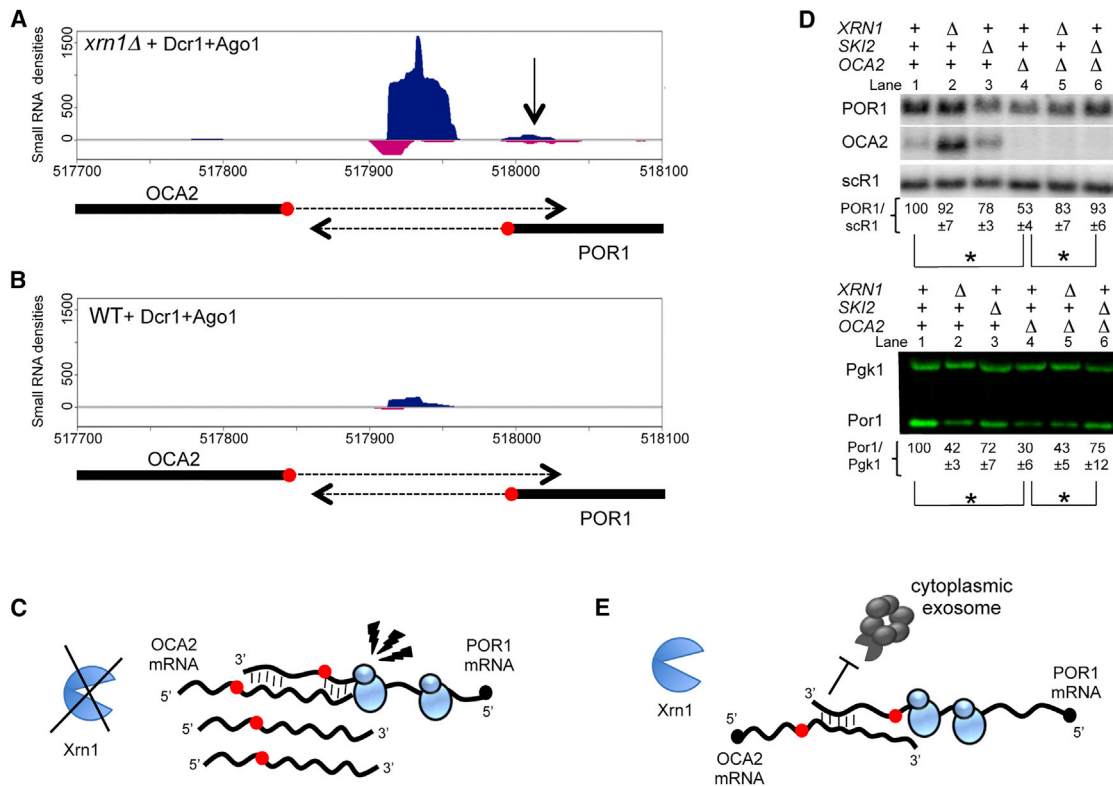
**Figure 4. Detection of Double-Stranded mRNA Duplexes in the *OCA2-POR1* Locus in Wild-Type and *xrn1Δ* Strains**

(A) Snapshot of the small RNA accumulation of 19–23 nucleotides within the OCA2-POR1 region in wild-type in the presence of Dcr1/Ago1. The arrow shows reads corresponding to the POR1 ORF.

(B) Snapshot as in (A) in the *xrn1* mutant. Small RNA reads originating from Watson strand are shown in blue, and small RNA reads originating from Crick strand are shown in red. Read densities are in linear scale. Dashed arrows represent the non-translated regions of the OCA2 and POR1 mRNAs, and filled boxes indicate ORFs. Chromosome 14 coordinates are indicated below (from 517700 to 518100).

(C) Model of the translational regulation of POR1 mRNA in the *xrn1* mutant. The ribosome stall due to the presence of OCA2-POR1 RNA duplex is symbolized by lightning flashes. This representation compiles information provided in Figures 2, 3, and 4A.

(D) Northern blot analysis of POR1 and OCA2 mRNAs (up panel) and corresponding western blot analysis of Por1 protein (down panel) in different *xrn1Δ*, *ski2Δ*, and *oca2Δ* genetic contexts. Quantifications of the POR1 mRNA, relative to scR1, are denoted as POR1/scR1. Quantifications of Por1 protein relative to Pgk1 as a loading control are denoted as Por1/Pgk1. Northern and western blot quantifications are indicated with SEs calculated from at least three independent experiments. Two-tailed t test statistics were used; * $p < 0.01$.

(E) Model of the functional stabilization of POR1 mRNA by OCA2 mRNA in wild-type cells. Interaction with the OCA2 mRNA protects the POR1 mRNA 3′ end against the exosome mediated 3′-5′ degradation. This representation compiles information provided in (B) and (C). Translational stop codons are indicated by red circles. Bars indicate the potential interactions between sequences of the two RNAs.

the production of GFP 3′ RNA fragments demonstrated that the c-mycGFP no. 1 mRNA was still an NGD substrate (Figure 3E, lane 6) whereas the c-mycGFP no. 2 mRNA was not (Figure 3E, lane 8). Taken together, these results show that mRNA-mRNA interactions exist in vivo and can have post-transcriptional outcomes, such as translation arrest and NGD.

**Small RNA Production from RNAi Competent *S. cerevisiae* Validates the Existence of OCA2-POR1 mRNA Interactions In Vivo**

To demonstrate the formation of RNA duplexes between OCA2 and POR1 mRNAs by an alternative method, we exploited an RNAi tool that has been previously reported to detect the genome-wide formation of RNA duplexes in yeast (Drinnenberg et al., 2009). RNAi, a gene-silencing pathway triggered by dou-

ble-stranded RNA, has been lost in the model budding yeast *S. cerevisiae*, but the introduction of Dicer (Dcr1) and Argonaute (Ago1) from *Saccharomyces castellii* leads to the production of artificial siRNAs. RNAi-competent *S. cerevisiae* thus allows the identification of small RNAs (19–23 nts), corresponding to naturally formed RNA duplexes in vivo (Drinnenberg et al., 2009; see Experimental Procedures). We therefore used this RNAi tool to determine the density of small RNAs produced in the presence or absence of Dcr1/Ago1 in both wild-type and *xrn1* mutant strains.

First, we compared the density of small (19- to 23-nt) RNAs corresponding to the *POR1-OCA2* locus produced in wild-type and *xrn1* mutant strains in the presence of Dcr1/Ago1. RNA duplexes between the 3′ UTR regions of these two RNAs were clearly observed in Xrn1-deficient cells and were also detectable in wild-type cells (Figures 4A and 4B). The data also show that

small RNAs extend into the POR1 open reading frame in the absence of Xrn1 (Figure 4A). This perfectly fits our previous conclusion that RNA duplexes exist within the POR1 ORF and block ribosome progression in Xrn1-deficient cells (Figure 4C).

These data also suggest that the OCA2 mRNA interacts with POR1 mRNA in wild-type cells, but these interactions appear restricted to the 3′ UTR regions (Figure 4B). We thus asked whether *POR1* expression would be affected by the absence of the OCA2 transcript in an XRN1+ background. Surprisingly, we observed that both POR1 mRNA and Por1 protein levels were significantly lower in the absence of OCA2 mRNA (*oca2Δ* strains; Figure 4D, lane 1 versus 4), suggesting a positive effect of OCA2 on POR1 functionality in wild-type cells. Additional deletion of *XRN1* increased POR1 mRNA levels slightly in the absence of OCA2 mRNA (Figure 4D, lane 5) but had no effect on protein levels. In contrast, deletion of *SKI2*, which inactivates the cytoplasmic 3′-5′ exonucleolytic activity of the exosome (Anderson and Parker, 1998), allowed a significant recovery of both POR1 mRNA and protein levels close to the levels observed in wild-type cells (Figure 4D, lane 6 versus 1). This suggests that the levels and translation of the POR1 mRNA are impacted by the cytoplasmic exosome in the absence of OCA2 mRNA. Thus, the role of OCA2 mRNA is different in wild-type cells versus *xrn1Δ* cells, in one case leading to the functional stabilization of the POR1 mRNA and, in the other, translational repression and NGD (Figure 4E versus Figure 4C).

We also determined whether blocking deadenylation, which is a prerequisite step before cytoplasmic 3′-5′ exonucleolytic degradation, would abolish the impact of the *OCA2* deletion. Indeed, we observed that Por1 protein levels were maintained and were unaffected by the absence of *OCA2* expression in the *ccr4* mutant in which deadenylation is impaired (Collart and Panasenko, 2012) (Figure S3, lane 6 versus 4). We therefore propose that the POR1 mRNA is normally targeted by 3′-5′ exonucleolytic attack. This is consistent with the classification of POR1 mRNA as a natural target of the exosome-dependent cytoplasmic mRNA decay pathway (Tuck and Tollervey, 2013). We additionally show that interaction with the OCA2 mRNA facilitates *POR1* expression. Thus, the OCA2 transcript naturally contributes to the functional stabilization of the POR1 mRNA in wild-type cells through an mRNA-mRNA interaction that is restricted to their 3′ UTRs. In addition, as we have seen, Xrn1 activity is important to limit the accumulation of the OCA2 message, because uncontrolled accumulation of OCA2 mRNA and extension of the hybrid into the POR1 ORF lead to translational repression of *POR1* and NGD.

### The Genome-wide Abundance of mimRNAs Is Controlled by Xrn1
We extended our analysis of the OCA2-POR1 locus to other convergent mRNA pairs. At a global scale, we analyzed 4,013 mRNAs, consisting of 2,557 annotated mRNAs with no obvious antisense RNA, which we called solo mRNAs, and 1,456 convergent and overlapping mRNAs (Table S1). For each of these mRNAs, we calculated the density of small RNAs produced in the presence or absence of Dcr1/Ago1 in both wild-type and *xrn1* mutant strains. Figures 5A and 5B reveal that solo RNAs were poor sources of small RNAs in the presence of Dcr1/

Ago1 and were not affected by the absence of Xrn1. In contrast, convergent mRNAs, overlapping either in their 3′ UTR region or also overlapping within their ORFs, were sensitive to the presence of Dcr1/Ago1 and produced an additional enrichment in small RNAs in the *xrn1* mutant (Figures 5A and 5B).

We pursued the analysis of small RNA data by representing each mRNA, either in the wild-type or in the *xrn1* mutant, by following the distribution of its small RNA density ratio (in the presence of Dcr1/Ago1 versus in the absence of Dcr1/Ago1) plotted against the average of its small RNA density (in the presence and in the absence of Dcr1/Ago1), a representation known as an MA plot (Figures 5C and 5D; Table S2; see Experimental Procedures). The MA plot showed that 33.6% of convergent mRNAs produced a ≥2-fold enrichment of small RNA levels in RNAi-competent wild-type cells (Figures 5C and 5E; Table S2). Remarkably, in the absence of Xrn1, we detected a massive enrichment of mRNA-mRNA interactions involving 678 mRNAs (62.4% of convergent mRNAs; Figures 5D and 5E; Tables S3 and S4).

### Validation of Two New mimRNA Pairs
To validate the existence of other no-go-decay-targeted mimRNAs, two pairs of convergent and 3′-overlapping mRNAs, SRB7-PMT7 (Figure 6A) and SNM1-PEX29 (Figure 6B), which show small RNA enrichment in the presence of Dcr1/Ago1 (Tables S3 and S4), were selected for further analysis. RNA duplexes between the 3′ UTR and ORF regions of these two RNAs in wild-type cells were observed and were strongly increased in Xrn1-deficient cells (Figure 6C shows *SRB7-PMT7* locus, and Figure 6D shows *SNM1-PEX29* locus). In the absence of Xrn1, we observed an accumulation of 3′ RNA fragments of the PMT7 mRNAs (Figure 6E) and SNM1 mRNAs (Figure 6F) that was dependent on the overexpression of SRB7 and PEX29 mRNAs, respectively. As for OCA2 and POR1, we conclude that these mRNA-mRNA interactions occur in vivo and are subjected to Xrn1 surveillance.

### DISCUSSION

In this work, we address the cytoplasmic fate of 3′-overlapping mRNAs that result from the transcription of convergent coding genes, specifically whether they can form mRNA duplexes with functional outcomes in vivo. We thus propose a post-transcriptional model as an alternative to one proposing that RNA polymerase (RNAP) collision regulates the expression of convergent genes at a transcriptional level (Prescott and Proudfoot, 2002). This is noteworthy because a recent study of 600 convergent transcript pairs with overlapping 3′ UTRs questioned the prevalence of the RNAP collision model in *S. cerevisiae* (Wang et al., 2014). In this study, the authors explored the regulation of the expression of specific convergent gene pairs but did not consider mRNA-mRNA interactions as a possible mechanism. We suspect that many of the mRNA pairs that they analyzed are mimRNAs. The regulation of the expression of these selected genes can be fully explained by the post-transcriptional effects we observed here.

The starting point of our study was that the defective *POR1* gene expression in Xrn1-deficient cells could not be explained by existing transcriptional models involving ncRNAs.
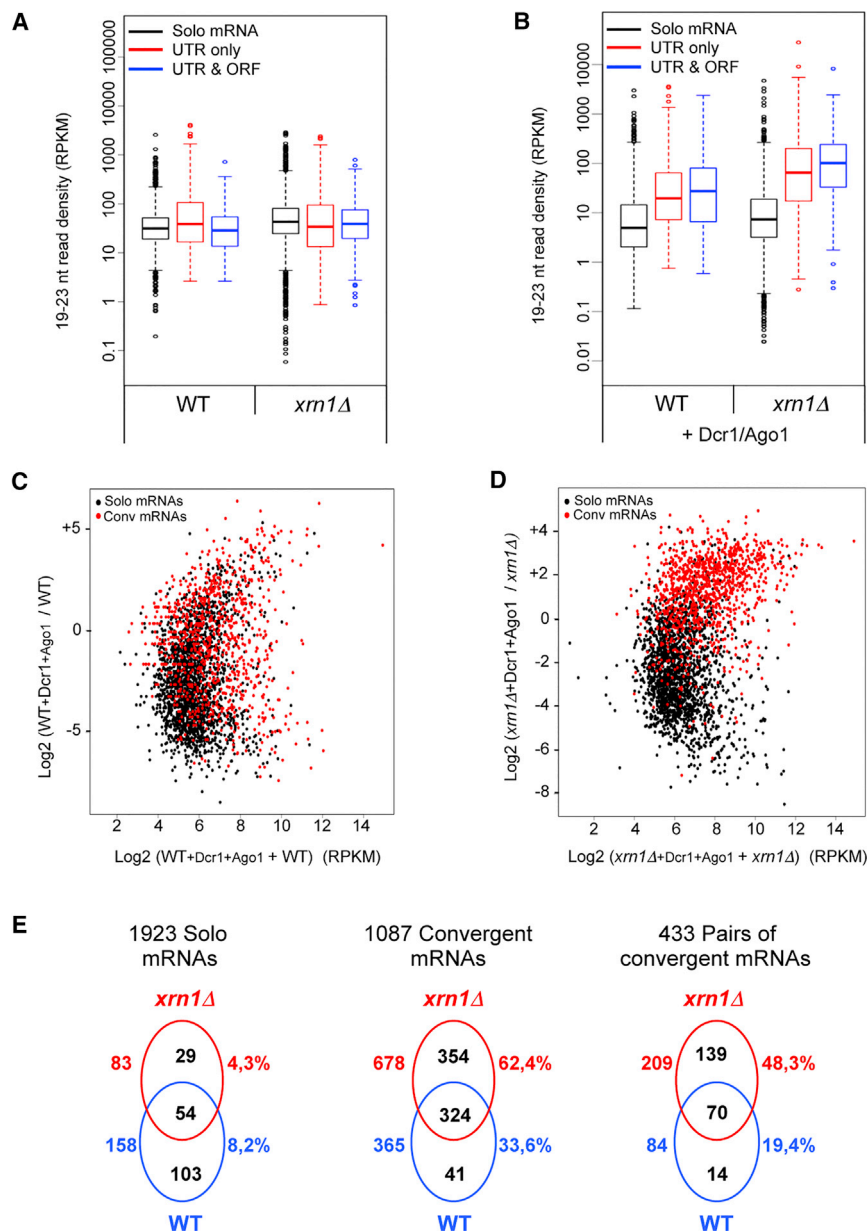
**Figure 5. Genome-wide Detection of Double-Stranded mRNA Duplexes in Wild-Type and *xrn1Δ* Strains**

(A) Boxplots showing the average density of 19–23 nucleotide tags within 3′-overlapping convergent genes and non-overlapping genes in the absence of Dcr1/Ago1 in the indicated strains. 4,013 mRNAs were defined (see Experimental Procedures and Table S1). 1,456 3′-overlapping convergent mRNAs and 2,557 mRNAs having no antisense (called solo mRNAs) were analyzed. Among convergent mRNAs, we defined 1,142 mRNAs overlapping in their 3′ UTR only (UTR only) and 315 overlapping within their ORF (ORF and UTR). Read densities are in rpkm (reads per kilobase of transcript per million mapped reads; see Table S1).

(B) Boxplots showing the average density of 19–23 nucleotide tags within 3′-overlapping convergent genes and non-overlapping genes as in (A) except for the presence of Dcr1/Ago1.

(C) MA plot representation of 19- to 23-nt small RNA density ratio in wild-type strains with or without Dcr1/Ago1 (labeled $Log_2$ [WT$_{+Dcr1+Ago1}$ /WT]) as a function of 19- to 23-nt small RNA density average in the same strains (labeled $Log_2$ [WT$_{+Dcr1+Ago1}$ + WT]). In this MA plot, 1,923 solo mRNAs (black dots) and 1,087 convergent mRNAs (conv mRNAs indicated by red dots) are represented after filtering out 1,003 mRNAs, corresponding to 25% of the 4,013 mRNAs showing the lowest small RNA density (see Figure S4 and Table S2).

(D) MA plot representation performed as in (C), in the *xrn1* mutant strain, with the same subset of mRNAs.

(E) Venn diagram representation of numbers and percentages of solo mRNAs, convergent mRNAs, or pairs having both convergent mRNAs showing ≥2-fold small RNA enrichment in the presence of Dcr1/Ago1 in the wild-type and in the *xrn1* mutant (data obtained from the MA plot analyses; see also Tables S3 and S4 for details).

inactivation of the cytoplasmic factor Ski2; Doma and Parker, 2006; Passos et al., 2009).

Importantly, we show that the levels of the POR1 3′ fragment increase when OCA2 mRNA is overproduced in *trans*. This *trans* effect allowed us to demonstrate clearly that these mRNAs interact in vivo. Indeed, expression of a set of mRNAs in *trans* with complementarity between their 3′ UTRs, their coding regions, or both showed that extensive complementarity and invasion of the coding sequence are required for NGD to occur. We can thus abolish or trigger the production of a 3′ fragment by disrupting or restoring a full complementarity between the 3′ regions of the two mRNAs, respectively. One important outcome of these experiments is the demonstration that NGD can be triggered by the expression of an antisense mRNA in *trans* and not solely by the presence of elements in *cis*, such as a stem-loop structure, rare codons, truncated mRNA, or mRNA depurination (Doma and Parker, 2007; Passos et al., 2009; Gandhi et al., 2008).

First, POR1 mRNAs were abundant and ribosome-associated in *xrn1* mutants, but the corresponding Por1 protein levels were very low, suggesting a post-transcriptional control mechanism. Second, accumulation of the 3′-overlapping OCA2 mRNA, whether in *xrn1* mutants or upon overexpression in *trans*, was associated with an additional decrease in Por1 protein production, suggesting that Por1 levels were regulated by the OCA2 mRNA. In this paper, we show that an mRNA-mRNA duplex forms in vivo, inhibits ribosome translocation on the POR1 mRNA, and triggers NGD (Doma and Parker, 2006). Consistent with the NGD pathway, a 3′ fragment of POR1 accumulates in an *xrn1Δ* mutant and is reduced in a *dom34Δ* mutant. Degradation of this fragment is completely independent of the cytoplasmic 3′-5′ mRNA decay pathway (i.e., unaffected by the
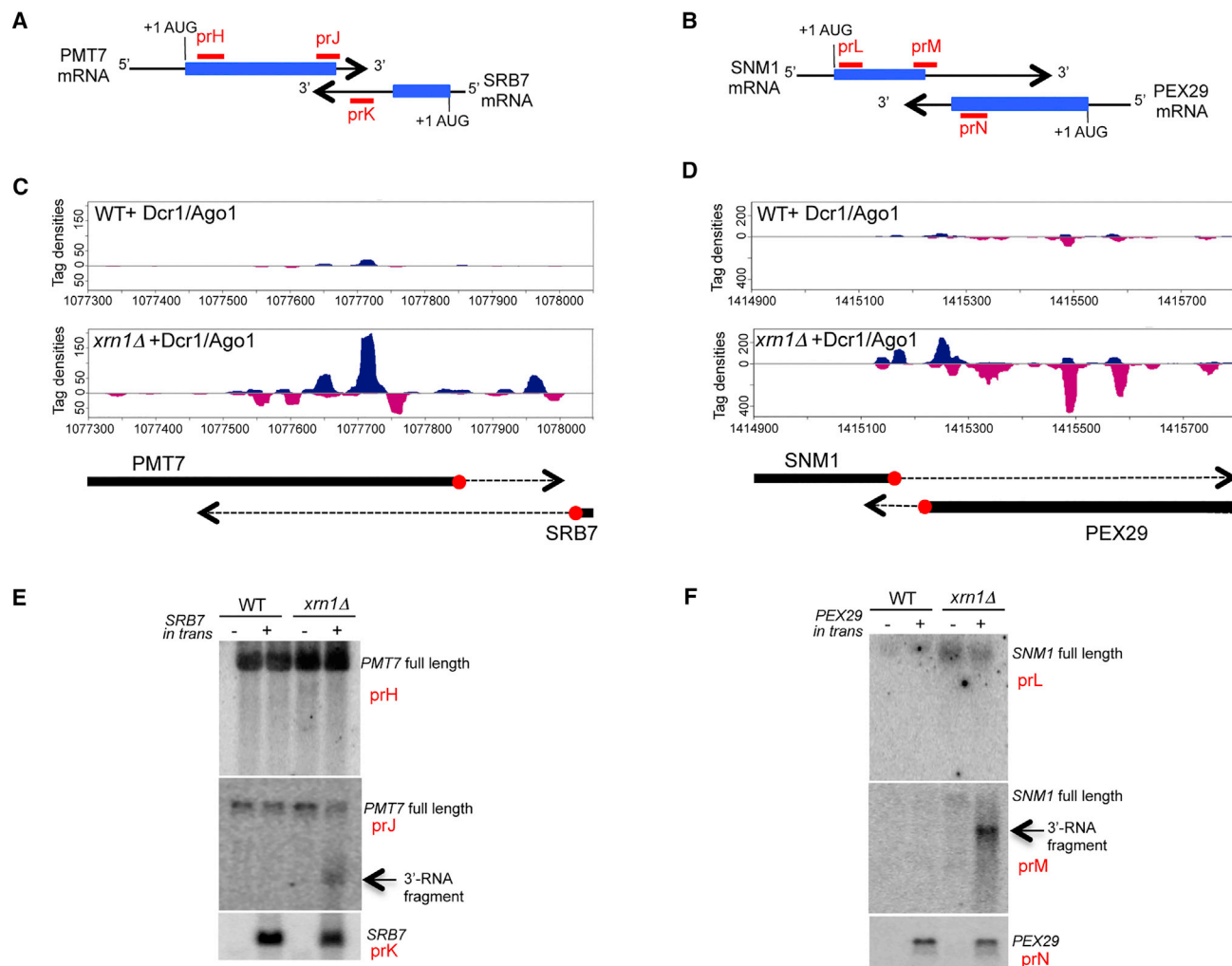
**Figure 6. Validation of Two New mimRNA Pairs**

(A) Schematic of the convergent PMT7 and SRB7 mRNA pair (YDR307W and YDR308C, respectively). These convergent mRNAs overlap and were shown to produce small RNA enrichment in the presence of Dcr1/Ago1 (Tables S3 and S4). Filled boxes indicate open reading frames, and black arrows represent 3′-non-translated regions of mRNAs. Specific probes prH, prJ, and prK used in northern blots are indicated in red.

(B) Schematic of convergent SNM1 and PEX29 mRNA pairs (YDR478W and YDR479C, respectively). Specific probes prL, prM, and prN used in northern blots are indicated in red.

(C) Snapshot of the small RNA accumulation of 19–23 nucleotides within the *PMT7-SRB7* region in wild-type and *xrn1* mutant strains in the presence of Dcr1/Ago1. Small RNA reads originating from Watson strand are shown in blue, and small RNA reads originating from Crick strand are shown in red. Read densities are in linear scale. Chromosome 4 coordinates are indicated below. Dashed arrows represent the non-translated regions of PMT7 and SRB7 mRNAs, and filled boxes indicate ORFs. Translational stop codons are indicated by red circles.

(D) Snapshot as in (C) of the small RNA accumulation of 19–23 nucleotides within the SNM1-PEX29 region.

(E) Northern blot analysis to detect the 3′ RNA fragment of PMT7 mRNA when SRB7 mRNA is expressed in *trans* (+) or not (−).

(F) Northern blot analysis to detect the 3′ RNA fragment of SNM1 mRNA when PEX29 mRNA is expressed in *trans* (+) or not (−).

Interestingly, sequence complementarity between the two mRNAs is not sufficient to induce NGD when this complementarity is limited to the ORF of the POR1 mRNA, i.e., the appearance of NGD fragments also requires a complementarity within the 3′ UTR. 3′ UTR regions are not associated with poly(A)-binding proteins, and cells actively control translational termination to keep this region free of ribosomes (Guydosh and Green, 2014). It is thus likely that the 3′ UTR is more accessible and facilitates the first step of mimRNA annealing. The 3′ UTR of POR1 mRNA likely

serves as a landing pad, and only subsequently would the stabilized RNA duplex extend within the ORF to promote inhibition of ribosome elongation.

Xrn1 has been recently implicated in regulating mRNA synthesis in the nucleus of *S. cerevisiae* (Haimovich et al., 2013; Sun et al., 2013), but the NGD signal that we observe constitutes an important indication that we are dealing with a cytoplasmic co-translational event dependent on Xrn1. This is also supported by RNAPII CHIP experiments showing that no difference in PolII

occupancy in the *POR1-OCA2* locus can be detected between WT and *xrn1Δ* strains (van Dijk et al., 2011). Here, we propose that the main cause of the low levels of Por1 protein in *xrn1Δ* strains is a translational defect due to a translation stop codon embedded in the RNA duplex and that NGD is provoked by a small subset of the stalled ribosomes. Indeed, only a small portion of the POR1 mRNA is cleaved when NGD occurs. The change in expression of two GFP mRNA reporters that differ only by an additional stop codon, causing termination of translation of upstream the RNA duplex, validates this translational mechanism.

The successful use of a set of artificial 3′ complementary mRNA regions to trigger NGD argues that the formation of mRNA-mRNA duplexes is not specific to the *POR1-OCA2* gene system. Our global approach using a previously developed RNAi tool confirms that this is a general phenomenon in *S. cerevisae* (Drinnenberg et al., 2009, 2011). Hundreds of additional pairs of 3′-overlapping mRNAs were found to be major sources of small RNAs in the RNAi-competent *xrn1* mutant. Based on the assumption that the small RNAs resulted from 3′ complementary mRNAs processed by Dcr1 in living cells, we conclude that these 3′-overlapping mRNAs co-exist within the same cell and that mRNA-mRNA interactions are a basic and general feature of convergent and 3′-overlapping mRNAs. In addition, we successfully verified that two other mRNAs, selected from this global approach, produce 3′ RNA NGD-like fragments in Xrn1-deficient cells. Thus, Xrn1 plays a key surveillance role in modulating post-transcriptional control of convergent gene expression, a new function for this enzyme.

One could argue that an active Xrn1 will degrade these potentially regulating mimRNAs and, as a consequence, some of these interactions will never occur in a wild-type context. Metagene representations of read distribution of small RNAs in mRNAs with overlapping 3′ UTRs only or overlapping ORFs and 3′ UTRs show clearly that the small RNA enrichment detected in the *xrn1* mutant is also visible in the wild-type (Figure 7). Therefore, the *xrn1* mutant simply amplifies the detection of interactions that are pre-existing in wild-type cells. The functional importance of these mRNA-mRNA interactions in wild-type cells was demonstrated by the fact that the presence of the OCA2 mRNA interferes with 3′–5′ mRNA degradation of the POR1 mRNA and leads to increased protein production. We therefore demonstrate that the modulation of convergent mRNA levels can have an important biological impact on gene expression at a post-transcriptional level in both wild-type and Xrn1-deficient cells. The logical extension of these conclusions is that physiological modulations of the synthesis or stability of 3′-overlapping mRNAs will affect the formation of the mRNA duplexes and trigger post-transcriptional processes. This is fully consistent with a previous analysis revealing that a significant number of convergent genes showed a pattern of negative correlation in expression across a broad range of growth conditions (Wang et al., 2014). Additionally, because the post-transcriptional effects are amplified in the absence Xrn1, it is also interesting to consider natural conditions in which Xrn1 activity is reduced in wild-type cells. In this regard, our observation of NGD for the *POR1-OCA2* gene pair in the presence of lithium, a stress condition known to inhibit Xrn1 activity (Dichtl et al., 1997; van Dijk et al., 2011), is significant.

We propose that the interactions detected between hundreds of mRNA pairs can participate in the modulation of diverse post-transcriptional events that could be specific to each mRNA pair and complex to decipher. Although factors associated with RNAi are not naturally present in *S. cerevisiae*, by analogy to what is known about miRNA function (Carthew and Sontheimer, 2009), we can imagine that mRNA-mRNA interactions might not only affect degradation and translation but also mask access to other regulators or participate in the re-localization of the mRNAs.

Interestingly, gene ontology (GO) analyses performed on 84 pairs of mimRNAs showing the strongest interactions (i.e., showing ≥2-fold small RNA enrichment) in the wild-type cells, and 209 pairs in the *xrn1* mutant (Table S4) highlighted a large set of genes involved in metabolic processes or associated with organellar or nuclear functions (Table S5). The number of genes forming a mimRNA pair and sharing the same process or component GO term is indicated in Table S5. Their existence unravels a potential co-regulatory phenomenon that could be mediated by these mRNA-mRNA interactions.

There is a broader implication that such mRNA-mRNA interactions will occur in other eukaryotes. The role of mRNA duplexes may be more complex in these cases because they can be recognized as dsRNAs and treated by Dcr1. The SRO5-P5CDH sense-antisense messenger pairs proposed to be processed into natural siRNAs in *A. thaliana* are one example (Borsani et al., 2005), but it is noteworthy that natural antisense transcripts in plants have been proposed to have a regulatory role that is not linked to double-stranded RNA degradation (Jen et al., 2005). In human cells, the RNA masking of splicing elements by mRNA-mRNA interactions is one example of Dcr1-independent regulation (Hastings et al., 1997). However, it is also possible to propose Dcr1-dependent effects and that mRNA duplexes are sources of siRNAs.

Interestingly, a study of five metazoan genomes concluded that the retention of some overlapping protein-coding gene pairs is not random but rather has evolutionary and functional significance (Soldà et al., 2008). In this regard, the fact that the evolutionarily conserved Xrn1 plays a key role in downregulating the phenomenon is significant. For instance, in addition to having many unexplained pleiotropic effects in yeast, Xrn1 homologs also have health and developmental importance in higher eukaryotes (Nagarajan et al., 2013). Whereas some of these defects may be directly explained by Xrn1's role in the 5′-3′ mRNA pathway of mRNA turnover of developmentally important mRNAs, it is also possible that some are caused via indirect effects on convergent gene transcripts as described here.

## EXPERIMENTAL PROCEDURES

### Yeast Media, Plasmids, Strains, and Oligonucleotides

The media, plasmids, strains of *S. cerevisiae,* and oligonucleotides used in this study are described in the Supplemental Experimental Procedures and Tables S6, S7, and S8, respectively.

### Northern Blot Analysis

RNA extracts and northern blots were performed as described previously (Sinturel et al., 2012). Blots were exposed to PhosphorImager screens, scanned using a Storm scanner (Molecular Dynamics), and quantified with ImageJ software.
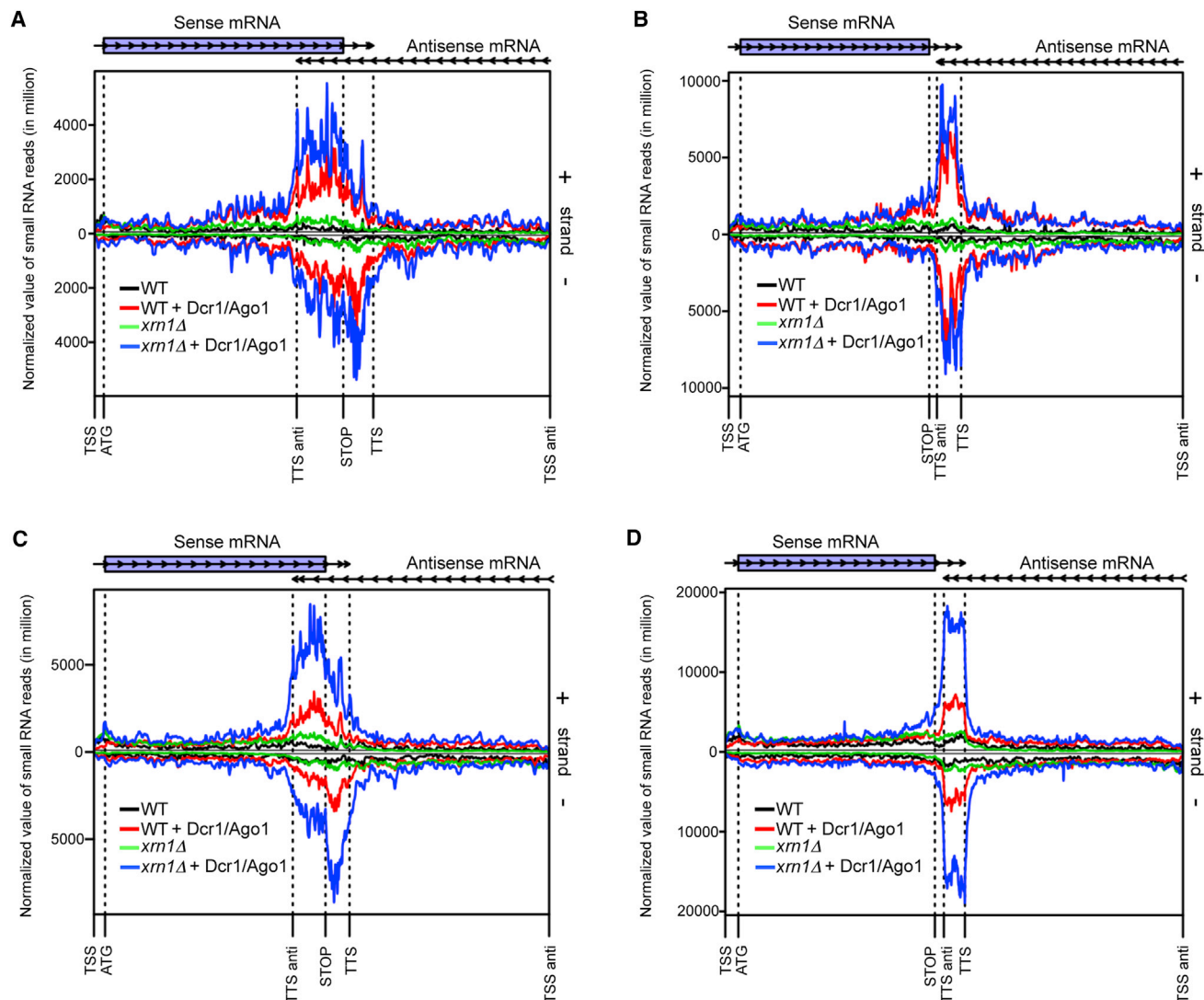
**Figure 7. Metagene Representations of Small RNA Reads on Different Pairs of Convergent mRNAs**

Analysis was performed for mRNAs showing ≥2-fold small RNA enrichment in the presence versus the absence of Dcr1/Ago1 in the indicated strains (see Tables S3 and S4 for details on selected mRNAs).

(A) Small RNA meta-signal along mRNAs overlapping within their ORF (ORF-UTR) and showing small RNA enrichment in both wild-type and *xrn1Δ* conditions (53 mRNA pairs analyzed).

(B) Same as (A) for mRNAs overlapping in their 3′ UTR only (UTR only; 87 mRNA pairs analyzed).

(C) Small RNA meta-signal along mRNAs overlapping within their ORF (ORF-UTR) and showing small RNA enrichment in the *xrn1* mutant only (127 mRNA pairs analyzed).

(D) Same as (C) for mRNAs overlapping in their 3′ UTR only (UTR only; 291 mRNA pairs analyzed). Above each panel, arrows represent sense and antisense mRNAs, and the ORF of the sense mRNA is indicated by a blue box. Different boundaries delimiting regions of interest are defined: sense mRNA transcription start site (TSS), translation start (ATG) and stop codon (STOP), and transcription termination site (TTS); antisense mRNA transcription termination site (TTS anti) and transcription start site (TSS anti). x and y axis correspond, respectively, to virtual nucleotides and to the mean of the normalized small RNA signal in rpkm at each virtual nucleotide (see Experimental Procedures for details).

### Polysome Analysis

This method has been described previously (Hu et al., 2009).

### Western Blot Analysis

Western blot was performed as described previously (Sinturel et al., 2012) with minor modifications indicated in the Supplemental Experimental Procedures.

### RNA-Sequencing of RNAi-Competent Cells

*S. cerevisiae* strains expressing Dcr1 and Ago1 are listed in Table S7. Small-RNA-seq libraries were constructed according to the Small RNA Sample Preparation Guide (Illumina) using 10- to 40-nt small RNAs purified from total RNA on 15% TBE-urea PAGE. Size selection was validated by qualitative analysis of a sample of the purified small RNA fraction on a Small RNA chip in a 2100 bioanalyzer (Agilent). Single-end sequencing (40 nt) of libraries

was performed on a Genome Analyzer IIx (Illumina). After removal of adaptor sequences using the Cutadapt tool (Martin, 2011), reads were uniquely mapped to the reference genome (*S. cerevisiae* S288C, 12/12/2011, retrieved from SGD; http://www.yeastgenome.org/) using version 0.12.7 of Bowtie (Langmead et al., 2009) with a tolerance of three mismatches. All subsequent bioinformatic analyses were performed using uniquely mapped 19- to 23-nt small RNA reads.

### Small RNA Analysis

4,013 mRNAs (after having excluded mRNAs with annotated antisense ncRNAs and dubious ORFs) were defined (Table S1). 1,456 convergent and 3′-overlapping mRNAs and 2,557 mRNAs having no antisense (called solo mRNAs) were analyzed. Among convergent mRNAs, we defined 1,142 mRNAs overlapping in their 3′ UTR only (UTR only) and 315 additionally overlapping within their ORF (ORF and UTR). Only $\geq$ 23-nt overlaps between two convergent mRNAs were considered. For convergent mRNAs, 19- to 23-nt small RNA reads were counted within the region of overlap, on the considered strand. For solo mRNAs, reads were counted within the full-length transcripts. For each gene class, total read counts were expressed in rpkm (reads per kilobase of transcript per million mapped reads). Annotations of UTRs were retrieved from the reference genome R63 and imported into our reference genome using Blastn alignments. For MA plot analysis, 1,923 solo mRNAs and 1,087 convergent mRNAs (red dots) are represented after filtering out the 1,003 mRNAs (25% of the 4,013 mRNA sets defined in Table S1), showing the lowest density average in the four strains (WT$_{+Dcr1+Ago1}$ + WT + xrn1$\Delta$ $_{+Dcr1+Ago1}$ + xrn1$\Delta$; Figure S4; see Table S2 for selected mRNAs).

### Metagene Representations

Metagenes of small RNA signal were generated using R scripts. Boundaries (TSS, ATG, STOP, TTS, TTS anti, and TSS anti) defined in Figure 7 delimited five regions of interest: region 1 from TSS to ATG (Figures 7A–7D); region 2 from ATG to STOP (Figures 7B and 7D) or from ATG to TTS anti (Figures 7A and 7C); region 3 from STOP to TSS anti (Figures 7B and 7D) or from TSS anti to STOP (Figures 7A and 7C); region 4 from TTS anti to TTS (Figures 7B and 7D) or from STOP to TTS (Figures 7A and 7C); and region 5 from TTS to TSS anti (Figures 7A–7D). We first determined the mean length $L$ of each region for each of the four subsets of genes analyzed in Figures 7A–7D. For regions 1–5 determined for Figure 7A, the mean length $L$ is 69, 1,464, 353, 228, and 1,341 nt, respectively; for regions 1–5 for Figure 7B, the mean length $L$ is 101, 1,614, 66, 207, and 1,896 nt, respectively; for regions 1–5 for Figure 7C, the mean length $L$ is 76, 1,280, 223, 164, and 1,361 nt, respectively; and for regions 1–5 for Figure 7D, the mean length $L$ is 97, 1,465, 67, 157, and 1,625 nt, respectively. Addition of the five $L$ values for each subset of genes gave the length in virtual nucleotides of the corresponding metagene. For each subset of genes, metagene was computed for each strain as follows. Signal for regions 1–5 was computed in rpkm for each $i$ gene ($i$ comprised between 1 and $n$). Each region was scaled to its corresponding $L$ value. Accordingly, signal associated to each nucleotide was scaled upon polynomial interpolation, so that each $j$ virtual nucleotide of the scaled region was associated to a scaled signal $S_{i,j}$. Scaled regions 1–5 were then concatenated, and $S_{i,j}$ values of all virtual nucleotides were summed to give $T_i$, corresponding to the whole signal for the $i$ gene. To ensure that each gene contributed equally to the final metagene, the $S_{i,j}$ value of the $j$ virtual nucleotide of the $i$ gene was divided by its associated $T_i$ value, giving a normalized $S_{i,j}^*$ signal for each position. Finally, the meta-signal at each $j$ virtual nucleotide was computed as $M_j = \left(\sum_{i=1}^{n} S_{i,j}^*\right) \times T/n$, where $T$ corresponds to the sum of the $T_i$ values of the $n$ genes of the subset.

### ACCESSION NUMBERS

A genome browser is publicly available at http://vm-gb.curie.fr/mimRNA/ (login: guest, password: sei:b7UM). RNA-seq data reported in this paper have been deposited to the NCBI GEO and are available under accession number GEO: GSE64090.

### SUPPLEMENTAL INFORMATION

Supplemental Information includes Supplemental Experimental Procedures, four figures, and eight tables and can be found with this article online at http://dx.doi.org/10.1016/j.celrep.2015.08.016.

### AUTHOR CONTRIBUTIONS

F.S., A.N., C.T., and L.B. designed, performed, and analyzed all experiments except for RNA-seq studies. M.W., M.D., and A.M. designed the RNA-seq procedure and performed and analyzed the RNA-seq data. L.B. conceived the project, analyzed all data, and wrote the manuscript.

### REFERENCES

Anderson, J.S., and Parker, R.P. (1998). The 3′ to 5′ degradation of yeast mRNAs is a general mechanism for mRNA turnover that requires the SKI2 DEVH box protein and 3′ to 5′ exonucleases of the exosome complex. EMBO J. *17*, 1497–1506.

Borsani, O., Zhu, J., Verslues, P.E., Sunkar, R., and Zhu, J.K. (2005). Endogenous siRNAs derived from a pair of natural cis-antisense transcripts regulate salt tolerance in Arabidopsis. Cell *123*, 1279–1291.

Carthew, R.W., and Sontheimer, E.J. (2009). Origins and Mechanisms of miRNAs and siRNAs. Cell *136*, 642–655.

Collart, M.A., and Panasenko, O.O. (2012). The Ccr4–not complex. Gene *492*, 42–53.

Dichtl, B., Stevens, A., and Tollervey, D. (1997). Lithium toxicity in yeast is due to the inhibition of RNA processing enzymes. EMBO J. *16*, 7184–7195.

Djebali, S., Davis, C.A., Merkel, A., Dobin, A., Lassmann, T., Mortazavi, A., Tanzer, A., Lagarde, J., Lin, W., Schlesinger, F., et al. (2012). Landscape of transcription in human cells. Nature *489*, 101–108.

Doma, M.K., and Parker, R. (2006). Endonucleolytic cleavage of eukaryotic mRNAs with stalls in translation elongation. Nature *440*, 561–564.

Doma, M.K., and Parker, R. (2007). RNA quality control in eukaryotes. Cell *131*, 660–668.

Drinnenberg, I.A., Weinberg, D.E., Xie, K.T., Mower, J.P., Wolfe, K.H., Fink, G.R., and Bartel, D.P. (2009). RNAi in budding yeast. Science *326*, 544–550.

Drinnenberg, I.A., Fink, G.R., and Bartel, D.P. (2011). Compatibility with killer explains the rise of RNAi-deficient fungi. Science *333*, 1592.

Faghihi, M.A., and Wahlestedt, C. (2009). Regulatory roles of natural antisense transcripts. Nat. Rev. Mol. Cell Biol. *10*, 637–643.

Gandhi, R., Manzoor, M., and Hudak, K.A. (2008). Depurination of Brome mosaic virus RNA3 in vivo results in translation-dependent accelerated degradation of the viral RNA. J. Biol. Chem. *283*, 32218–32228.

Guydosh, N.R., and Green, R. (2014). Dom34 rescues ribosomes in 3′ untranslated regions. Cell *156*, 950–962.

Haimovich, G., Medina, D.A., Causse, S.Z., Garber, M., Millán-Zambrano, G., Barkai, O., Chávez, S., Pérez-Ortín, J.E., Darzacq, X., and Choder, M. (2013). Gene expression is circular: factors for mRNA degradation also foster mRNA synthesis. Cell *153*, 1000–1011.

Hastings, M.L., Milcarek, C., Martincic, K., Peterson, M.L., and Munroe, S.H. (1997). Expression of the thyroid hormone receptor gene, erbAalpha, in B lymphocytes: alternative mRNA processing is independent of differentiation but correlates with antisense RNA levels. Nucleic Acids Res. *25*, 4296–4300.

He, F., Li, X., Spatrick, P., Casillo, R., Dong, S., and Jacobson, A. (2003). Genome-wide analysis of mRNAs regulated by the nonsense-mediated and 5′ to 3′ mRNA decay pathways in yeast. Mol. Cell *12*, 1439–1452.

Hu, W., Sweet, T.J., Chamnongpol, S., Baker, K.E., and Coller, J. (2009). Co-translational mRNA decay in Saccharomyces cerevisiae. Nature *461*, 225–229.

Jacquier, A. (2009). The complex eukaryotic transcriptome: unexpected pervasive transcription and novel small RNAs. Nat. Rev. Genet. *10*, 833–844.

Jen, C.H., Michalopoulos, I., Westhead, D.R., and Meyer, P. (2005). Natural antisense transcripts with coding capacity in Arabidopsis may have a regulatory role that is not linked to double-stranded RNA degradation. Genome Biol. *6*, R51.

Kapranov, P., Willingham, A.T., and Gingeras, T.R. (2007). Genome-wide transcription and the implications for genomic organization. Nat. Rev. Genet. *8*, 413–423.

Katayama, S., Tomaru, Y., Kasukawa, T., Waki, K., Nakanishi, M., Nakamura, M., Nishida, H., Yap, C.C., Suzuki, M., Kawai, J., et al.; RIKEN Genome Exploration Research Group; Genome Science Group (Genome Network Project Core Group); FANTOM Consortium (2005). Antisense transcription in the mammalian transcriptome. Science *309*, 1564–1566.

Langmead, B., Trapnell, C., Pop, M., and Salzberg, S.L. (2009). Ultrafast and memory-efficient alignment of short DNA sequences to the human genome. Genome Biol. *10*, R25.

Lapidot, M., and Pilpel, Y. (2006). Genome-wide natural antisense transcription: coupling its regulation to its different regulatory mechanisms. EMBO Rep. *7*, 1216–1222.

Li, J.T., Zhang, Y., Kong, L., Liu, Q.R., and Wei, L. (2008). Trans-natural antisense transcripts including noncoding RNAs in 10 species: implications for expression regulation. Nucleic Acids Res. *36*, 4833–4844.

Martin, M. (2011). Cutadapt removes adapter sequences from high-throughput sequencing reads. EMBnet.journal *18*, 10–12.

Munroe, S.H., and Zhu, J. (2006). Overlapping transcripts, double-stranded RNA and antisense regulation: a genomic perspective. Cell. Mol. Life Sci. *63*, 2102–2118.

Nagarajan, V.K., Jones, C.I., Newbury, S.F., and Green, P.J. (2013). XRN 5′ → 3′ exoribonucleases: structure, mechanisms and functions. Biochim. Biophys. Acta *1829*, 590–603.

Passos, D.O., Doma, M.K., Shoemaker, C.J., Muhlrad, D., Green, R., Weissman, J., Hollien, J., and Parker, R. (2009). Analysis of Dom34 and its function in no-go decay. Mol. Biol. Cell *20*, 3025–3032.

Pelechano, V., and Steinmetz, L.M. (2013). Gene regulation by antisense transcription. Nat. Rev. Genet. *14*, 880–893.

Pelechano, V., Wei, W., and Steinmetz, L.M. (2013). Extensive transcriptional heterogeneity revealed by isoform profiling. Nature *497*, 127–131.

Ponting, C.P., Oliver, P.L., and Reik, W. (2009). Evolution and functions of long noncoding RNAs. Cell *136*, 629–641.

Prescott, E.M., and Proudfoot, N.J. (2002). Transcriptional collision between convergent genes in budding yeast. Proc. Natl. Acad. Sci. USA *99*, 8796–8801.

Salato, V.K., Rediske, N.W., Zhang, C., Hastings, M.L., and Munroe, S.H. (2010). An exonic splicing enhancer within a bidirectional coding sequence regulates alternative splicing of an antisense mRNA. RNA Biol. *7*, 179–190.

Sanna, C.R., Li, W.H., and Zhang, L. (2008). Overlapping genes in the human and mouse genomes. BMC Genomics *9*, 169.

Sinturel, F., Bréchemier-Baey, D., Kiledjian, M., Condon, C., and Bénard, L. (2012). Activation of 5′-3′ exoribonuclease Xrn1 by cofactor Dcs1 is essential for mitochondrial function in yeast. Proc. Natl. Acad. Sci. USA *109*, 8264–8269.

Soldà, G., Suyama, M., Pelucchi, P., Boi, S., Guffanti, A., Rizzi, E., Bork, P., Tenchini, M.L., and Ciccarelli, F.D. (2008). Non-random retention of protein-coding overlapping genes in Metazoa. BMC Genomics *9*, 174.

Sun, M., Schwalb, B., Pirkl, N., Maier, K.C., Schenk, A., Failmezger, H., Tresch, A., and Cramer, P. (2013). Global analysis of eukaryotic mRNA degradation reveals Xrn1-dependent buffering of transcript levels. Mol. Cell *52*, 52–62.

Tuck, A.C., and Tollervey, D. (2013). A transcriptome-wide atlas of RNP composition reveals diverse classes of mRNAs and lncRNAs. Cell *154*, 996–1009.

van Dijk, E.L., Chen, C.L., d'Aubenton-Carafa, Y., Gourvennec, S., Kwapisz, M., Roche, V., Bertrand, C., Silvain, M., Legoix-Né, P., Loeillet, S., et al. (2011). XUTs are a class of Xrn1-sensitive antisense regulatory non-coding RNA in yeast. Nature *475*, 114–117.

Wang, X.J., Gaasterland, T., and Chua, N.H. (2005). Genome-wide prediction and identification of cis-natural antisense transcripts in Arabidopsis thaliana. Genome Biol. *6*, R30.

Wang, L., Jiang, N., Wang, L., Fang, O., Leach, L.J., Hu, X., and Luo, Z. (2014). 3′ Untranslated regions mediate transcriptional interference between convergent genes both locally and ectopically in Saccharomyces cerevisiae. PLoS Genet. *10*, e1004021.

Wilkening, S., Pelechano, V., Järvelin, A.I., Tekkedil, M.M., Anders, S., Benes, V., and Steinmetz, L.M. (2013). An efficient method for genome-wide polyadenylation site mapping and RNA quantification. Nucleic Acids Res. *41*, e65.

Wolin, S.L., and Walter, P. (1988). Ribosome pausing and stacking during translation of a eukaryotic mRNA. EMBO J. *7*, 3559–3569.

Yelin, R., Dahary, D., Sorek, R., Levanon, E.Y., Goldstein, O., Shoshan, A., Diber, A., Biton, S., Tamir, Y., Khosravi, R., et al. (2003). Widespread occurrence of antisense transcription in the human genome. Nat. Biotechnol. *21*, 379–386.

Zhang, Y., Liu, X.S., Liu, Q.R., and Wei, L. (2006). Genome-wide in silico identification and analysis of cis natural antisense transcripts (cis-NATs) in ten species. Nucleic Acids Res. *34*, 3465–3475.